UNCLASSIFIED

AD 269 769

Reproduced
by the

ARMED SERVICES TECHNICAL INFORMATION AGENCY
ARLINGTON HALL STATION
ARLINGTON 12, VIRGINIA

UNCLASSIFIED

METALLURGY

DEPARTMENT OF METALLURGY

Institute of Metals and Explosives Research

UNIVERSITY OF UTAH
SALT LAKE CITY, UTAH

INVESTIGATION OF HIGH VELOCITY IMPACT
AND SOME HIGH EXPLOSIVES PHENOMENA
FINAL REPORT

CONTRACT AF-18(603)-100   File 11-17-W

1 December 1961

Project Director: M. A. Cook
Report prepared by: R. T. Keyes

ABSTRACT

A brief summary of the important results obtained under Contract AF-18 (603)-100 is given. The subject matter covered by the investigations included: (1) high explosive generators for fast particles, (2) mechanism of cratering in ultra high velocity impact, (3) observations of vaporization accompanying ultra high velocity impact, (4) mechanism for crater expansion in shaped change penetration, (5) ionization and electron densities in detonating solid explosives, (6) electrical fields and electromagnetic radiation from chemical detonations, (7) external detonation generated plasmas, (8) the effect of pressure on the degree of ionization in gaseous detonations, (9) ionization and electrical conductivity and its relationship to the deflagration to detonation transition in solid explosives, and (10) transition to detonation in liquid explosives.

INVESTIGATIONS OF HIGH VELOCITY IMPACT AND SOME HIGH EXPLOSIVES PHENOMENA

I. Introduction

The following constitutes the final report on Contract AF-18(603)-100 entitled "Investigation of High Velocity Impact and Some High Explosives Phenomena". Work commenced on the contract 1 July 1955 and continued until 30 September 1961. The investigations carried out during this period may be considered to fall under the following general classifications: (1) high explosive generators for fast particles, (2) mechanism of cratering in ultra-high velocity impact, (3) observations of vaporization accompanying ultra-high velocity impact, (4) mechanism for crater expansion in shaped charge penetration, (5) ionization and electron densities in detonating solid explosives, (6) electrical fields and electromagnetic radiation from chemical detonations, (7) external detonation generated plasmas, (8) the effect of pressure on the degree of ionization in gaseous detonations, (9) ionization and electrical conductivity and its relationship to the deflagration to detonation transition in solid explosives, and (10) transition to detonation in liquid explosives.

The following constitutes the list of technical notes which have been published as a result of research on these subjects:

Technical reports originating from work under Contract AF-18(603)-100:

1. "Measurements of Ionization and Electron Densities in the Detonation Waves of Solid Explosives", Report #1, September 15, 1956.

2. "Behavior of Metals under Impact Loading and the Mechanism of Cratering", Report #2, October 15, 1956.

3. "Mechanism of Cratering in Ultra-High Velocity Impact", 10 July 1957, AFOSR-TN-57-486, AD 136 479.

4. "The Generation of High Velocity Projectiles with High Explosives", AFOSR-TN-57-696, AD 136 899, 1 October 1957.

5. "Propagation Characteristics of Detonation Generated Plasmas", AFOSR-TN-58-754, AD 201 613, 20 June 1958.

6. "Mechanism of Cratering in Ultra-High Velocity Impact", AFOSR-TN-59-50, AD 209 413, 30 January 1959.

7. "Electrical Fields and Electromagnetic Radiation from Chemical Explosions", AFOSR-TN-59-551, AD 216 691, 19 March 1959.

8. "Observations of Vaporization Accompanying Ultra-High Velocity Impact", AFOSR-TN-60-327, 4 January 1960.

9. "Framing Camera Observations of Ultra-High Velocity Penetration in Transparent Targets and a Mechanism of Crater Expansion", AFOSR-TN-60-851, 31 March 1960.

10. "Detonation Generated Plasmas", AFOSR-705, January 24, 1961.

11. "The Effect of Pressure on Ionization in Gaseous Detonation", AFOSR-704, March 31, 1961.

12. "Ionization Waves from Free Surfaces of Detonating Explosives", AFOSR-1335, September 7, 1961.

Publications based upon information given in the technical reports are as follows:

1. "Generation of High Velocity Projectiles", M. A Cook and R. T. Keyes, J. Appl. Phys., _29_, 1651 (1958).

2. "Mechanism of Cratering in Ultra-High Velocity Impact", M. A. Cook, J. Appl. Phys., _30_, No. 5, 725 (1959).

3. "Propagation Characteristics of Detonation-Generated Plasmas", M. A. Cook, R. T. Keyes and L. L. Udy, J. Appl. Phys., _30_, No. 12, 1881 (1959).

4. "Detonation-Generated Plasmas", A. Bauer, M. A. Cook and R. T. Keyes, Proc. Roy. Soc., Vol. A259, 508 (1961).

5. "Microsecond Framing Camera Photographs of High Velocity Impact", M. A. Cook and R. T Keyes, Paper presented at the Third Symposium on Hypervelocity Impact, Chicago, Illinois, October 7-9, 1958.

6. "Framing Camera Observations of Ultra-High Velocity Penetration in Transparent Targets and a Mechanism of Crater Expansion", R. W. Bartlett, M. A. Cook, and R. T. Keyes, Paper presented at the Fourth Symposium on Hypervelocity Impact, Eglin Air Force Base, April 27-28, 1960.

7. "Ionization Waves from Free Surfaces of Detonating Explosives", A. Bauer, M. A. Cook and L. A. Rogers, Paper presented at the Western States Section of the Combustion Institute, Berkley, California, September 7-8, 1961.

II. Summary of Results

A. High Explosive Generators for Fast Particles

The developments under this phase have been described in item #4 of the list of technical notes. The method which evolved employed 5 cm diameter Composition B

charges containing wave control inserts, Fig. 1 being a diagram of the basic charge. The wave control insert consisted of an 80° apex cone of height 2.5 cm which was composed of inert material. It was expected that the most suitable material
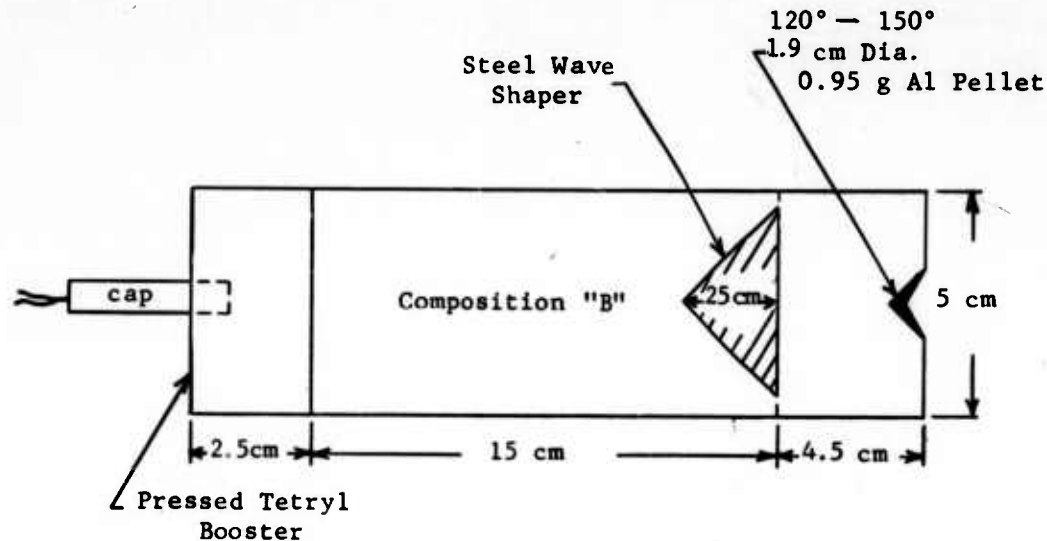

Figure 1. Basic charge used in the wave shaping method of accelerating projectiles.

from which to fabricate this cone would be glass. However, steel proved to be slightly superior, probably for the reason that the cones could be fabricated with more precision when made of steel. The precision of the charge components was found to be a very important factor affecting the performance. The function of the wave control insert was to produce an inverted detonation wave (concave-shaped looking from the front) rather than the usual spherical shaped wave (convex toward the front). The above type wave control insert in contrast to more bulky "interrupter type" wave shapers which shape the wave by stopping detonations completely beyond the insert, after which the wave is reformed by detonation of the explosive around the sides of the insert, permits initiation of detonation by the shock propagating through the insert. With such a device the variable delay desired across the wave front was produced by a combination of two factors. Firstly, because the detonation velocity of Composition B exceeded the velocity of the compressional wave generated in wave shaper, the wave was delayed progressively more toward the axis as the path length through the shaper increased. The second contribution resulted from the variable delaying of initiation of the explosive in the wafer beyond the wave

4-

control insert, the delay of initiation increasing as the path length through the wave shaper increased which resulted because the attenuation of the wave was greater. When wave shaping is accomplished in this manner the impulse of the detonation wave does not appear to be degraded to any great extent as in the case for "interrupter type" wave shapers where the detonation wave has to reform completely.

The benefit of such an "inverted" wave for accelerating projectiles was believed to be twofold. Firstly, an inverted detonation wave is unstable. The wave rapidly reverts to the normal spherical, convex shape by virtue of an increased velocity along the central part of the wave, and consequently the pellet is accelerated by a wave traveling at a velocity higher than the normal detonation velocity. Secondly, an inverted wave was found to lead to reduced fragmentation of the pellet.

Tests were carried out firstly to determine the most suitable shaped pellet, i.e., the shape primarily which possessed the smallest tendency to fragment. The best combination was found to be a 120° - 150° pellet (interior angle rear surface 120° - front surface 150° concave inward) or Pugh type fragment. Nextly, using 0.95 g, 1.9 cm diameter aluminum pellets of this type and 80° 2.5 cm height conical shaped wave control inserts the wafer length x (and consequently the shape of the wave impacting the pellet) was varied to determine the influence upon projectile velocity and projectile fragmentation. Fortunately, the tendency for projectiles to fragment appeared to be minimum for the wafer length that led to the highest velocities which was about 4.5 cm using either glass or steel wave control inerts. Under these optimum conditions velocities up to 7600 m/sec were realized with the 0.95 g aluminum pellets.

B. Mechanism of Cratering in Ultra-High Velocity Impact

This subject was treated in items #3 and #6 of the list of technical notes. Briefly, cratering was classified into three regions according to the striking velocity, as follows:

a. Impact at a striking velocity V in the range $V_\sigma > V > C$ where C is sonic velocity in the target and V_σ is the threshold velocity required to cause plastic deformation, i.e., the velocity at which the Bernoulli pressure, $1/2 \, \rho_p (V-U)^2$ is just equal to the yield strength σ, ρ_p being the density of the projectile and U the penetration velocity. This condition is possible only when $V_\sigma > C$ which requires generally a relatively low acoustic velocity such as a loose sand target.

b.   Impact at a striking velocity, V, such that $V_\sigma < V < V_{ct}$ where V_{ct} is the minimum velocity required for an impact explosion of the target, i.e., vaporization of the target. The type (b) penetration (with $V_\sigma < C$) is probably best known from studies of penetration of targets by shaped charge jets. This type cratering has been treated by applying the laws of hydrodynamics and considering the collision process under the approximation of non-viscous fluid flow.

c.   Cratering with $V > V_{ct}$. Impact explosions were expected to occur only for striking velocities somewhat above V_σ and C.

The type (a) penetration was not treated further in our studies. However, the idealized theory of type (b) penetration was reviewed, and then the principle of conservation of momentum was applied in a new way, yielding in the case of penetration by shaped charge jets an expression for the final crater diameter. The reasoning was as follows: During an infinitesmal increment of penetration δP which occurs during the time δt a total impulse

$$\delta I = 1/2 \lambda \rho_j (V_o - U_o)^2 A_o \delta t \tag{1}$$

is imparted to the target where ρ_j is the density of the jet, V_o is the jet velocity, U_o is the penetration velocity, A_o is the cross-sectional area of the jet, and λ is a factor to account for gaps between particles in a discontinuous jet. (For a continuous jet $\lambda = 1$.) The relation $1/2 \lambda \rho_j (V_o - U_o)^2$ is simply the Bernoulli pressure generated by a jet of velocity V_o in fluid flow penetrating a target at velocity U_o. Except at the surface of the target where relief of pressure allows some backward flow, this increment of impulse produces effectively only lateral residual flow. Since the area resisting the pressure of the lateral residual flow at the collision interface according to this concept is A_o, it was natural to conclude that the area resisting the lateral residual flow at a particular site may be taken to be A, the expanding cross-sectional area of the crater at the particular location where the increment of impulse was first received. Thus,

$$\delta I = 1/2 \lambda \rho_j (V_o - U_o)^2 A_o \delta t = (1/2 \rho_t U^2 + \sigma) A \delta t \tag{2}$$

where the zero subscripts indicate initial conditions. The expression $(1/2 \rho_t U^2 + \sigma)$ is simply the pressure of lateral residual flow, ρ_t being the target density, σ the dynamic yield strength of the target and U the lateral flow velocity at the crater location whose instantaneous cross-sectional area is A.

The crater will continue to expand until $U = 0$, i.e., until the pressure of lateral residual flow equals the static yield strength of the target, σ'. Setting $U = 0$, $\sigma = \sigma'$, eliminating U_o, and expressing cross-sectional areas of the crater and jet in terms of their diameters led to the expression

$$d' = \frac{d_o \rho_t^{1/2} (\lambda \rho_j)^{1/2}}{(\rho_j^{1/2} + \rho_t^{-/2})(2\sigma')^{1/2}} \, V_o \tag{3}$$

for the final crater diameter in terms of the jet diameter, d_o.

An expression for crater volume in single particle type (b) impact was developed where the energy radiated from the collision zone by shock waves was neglected. The development was based upon the idealized situation under which a target was considered to be penetrated by a cylindrical projectile of length L_p and diameter d_p. Under these conditions a cylindrical crater of constant radius would be formed, the radius of which could be calculated by means of equation 3. With the depth of penetration being given by

$$P = L_p (\rho_p/\rho_t)^2 \tag{4}$$

which is a well-known equation from shaped charge theory. The crater volume was then derived to be

$$\tau = \frac{\rho_p^{1/2} \rho_t^{1/2}}{(\rho_p^{1/2} + \rho_t^{1/2})^2} \frac{m_p V^2}{2\sigma} \tag{5}$$

which for $\rho_p = \rho_t$ reduced to

$$\tau = \frac{m_p V^2}{8\sigma} \tag{6}$$

where m_p is the projectile mass, V its velocity, and σ the yield strength of the target. For a spherical particle the impulse flow of the target would be radial and the resulting crater nearly hemispherical. However, it was concluded that the geometry of the dynamic pressure to static pressure conversion should be such that equations (5) and (6) should apply for spherical particles also.

Type (c) cratering was then discussed and predictions were made concerning the threshold velocity V_{ct} required for impact explosions. It was considered that the impact velocity V_{ct} would be such a velocity that the heat developed by inelastic collision in the target equaled the heat of vaporization, and that in general the penetration velocity U would be greater than the shock velocity corresponding to the Bernoulli pressure at the collision interface, i.e., the shock

wave would not move away from the collision interface, and thus there would be no means of removing from the target the heat of inelastic impact.

Through application of a theory for the compressibility of solids[1] the specific compressional work of inelastic impact was calculated in terms of the impact velocity and equated to the heat of vaporization to yield an expression for V_{ct}, the threshold velocity for vaporization, the result being

$$V_{ct} = \left[\frac{8h_c \rho_t}{\beta_o \rho_p^2} \right]^{-1/4} \frac{\rho_t^{1/2} + \rho_p^{1/2}}{\rho_t^{1/2}} \tag{7}$$

which for equal target and projectile materials reduces to

$$V_{ct} = 2(8h_c/\beta_o \rho)^{1/4} \tag{8}$$

where h_c is the specific heat of vaporization and β_o is the compressibility at atmospheric pressure. Some typical values of V_{ct} for various projectile-target combinations calculated by means of these equations are listed in Table 1.

Loss of energy from the material of the target, which is at any instant in collision with the projectile by means of the shock wave, was considered to occur only when $U < V_{st}$ where U is the penetration velocity and V_{st} is the velocity of the shock wave in the target. Therefore, the radiated shock waves should tend to prevent an impact explosion as long as the condition $U < V_{st}$ maintains. This situation was not considered to apply to projectiles, however, because shock waves propagating back into the projectile from the collision zone would not remove the inelastic impact energy from the projectile. On the basis of the assumption that the energy accumulated in the projectile part of the collision zone plus that which flowed away from the collision zone into the projectile was approximately the same as the energy accumulating in the target material plus that which flowed into the target in radiated shock waves, calculations showed that projectile impact explosions could possibly occur at velocities only about 45% of those required to produce target impact explosions.

An expression was next derived for the maximum amount of material which would be vaporized from a target. In the case of equal target and projectile materials the relationship in terms of the ratio of the mass of target material vaporized to the projectile mass was

$$m_t/m_p \leq \frac{v^2}{8h_c} - 1 \tag{9}$$

Table I: Critical impact and penetration velocities for target impact explosions

Projectile	Target	h_c Kcal/g	β_o atm$^{-1}\cdot 10^7$	P_{ct} megabars	V_{ct} km/sec	U_{ct} km/sec
Steel	Steel	1.7	5.94	1.37	11.8	5.9
Aluminum	Aluminum	2.04	13.85	0.58	13.0	6.5
Copper	Copper	1.28	7.27	1.14	10.0	5.1
Magnesium	Magnesium	1.50	29.5	0.27	11.2	5.6
Zinc	Zinc	0.41	13.0	0.43	7.0	3.5
Lead	Lead	0.23	24.2	0.30	4.6	2.3
Steel	Aluminum			0.58	10.3	6.5
"	Copper			1.14	10.4	5.1
"	Magnesium			0.27	8.2	5.6
"	Zinc			0.43	6.8	3.5
"	Lead			0.30	5.1	2.3
Aluminum	Steel			1.37	16.0	5.9
"	Copper			1.14	14.4	5.1
"	Magnesium			0.27	10.1	5.6
"	Zinc			0.43	9.2	3.5
"	Lead			0.30	7.0	2.3
Copper	Steel			1.37	11.4	5.9
"	Aluminum			0.58	18.0	6.5
"	Magnesium			0.27	8.1	5.6
"	Zinc			0.43	6.6	3.5
"	Lead			0.30	4.9	2.3
Magnesium	Steel			1.37	18.5	5.9
"	Aluminum			0.58	14.6	6.5
"	Copper			1.14	16.6	5.1
"	Zinc			0.43	10.6	3.5
"	Lead			0.30	8.2	2.3
Zinc	Steel			1.37	12.1	5.9
"	Aluminum			0.58	10.5	6.5
"	Copper			1.14	10.8	5.1
"	Magnesium			0.27	8.4	5.6
"	Lead			0.30	5.2	2.3
Lead	Steel			1.37	10.8	5.9
"	Aluminum			0.58	9.7	6.5
"	Copper			1.14	9.6	5.1
"	Magnesium			0.27	7.8	5.6
"	Zinc			0.43	6.3	3.5

C = velocity of sound = 5.3 (steel); 5.1 Al); 3.6 (Cu); 3.7 (Zn); 1.23 (Pb); 4.6 km/sec (Mg).

The second paper concerned with the mechanism of cratering in ultra-high velocity impact, i.e., item #6 on the list of technical notes, was concerned mainly with theoretical evaluations of dissipative factors occurring in the cratering process and the effect upon the idealized theory discussed in the preceding paper. In the non-idealized case under the conditions of plastic flow continuity of pressure at the impact junction between the projectile and the target may be expressed by the equation

$$\rho_p \ (V-U)^2/2 = \rho_t U^2/2 + \phi (U,\sigma) \tag{10}$$

where $\phi (U,\sigma)$ is a function describing dissipative pressures, e.g., losses associated with yield strength, compression, heating of the target, radiating shock waves, and possibly impact explosions. The term ϕ was therefore the dynamic yield strength of the target. The penetration equations for shaped charge jets were then derived for the non-idealized case, namely

$$U = V \ \{ 1 - [\Delta + 2\phi/\rho_j \ V^2 \ (1-\Delta)]^{1/2}/(1-\Delta)\} \tag{11}$$

and

$$P = \frac{L \ \{ \ 1-[\ \Delta+ \ 2\phi/ \ _j V^2 \ (1-\Delta)]^{1/2}}{[\Delta+ \ 2\phi/ \ _j V^2 \ (1-\Delta)]^{1/2} \ - \ \Delta} \tag{12}$$

$$\Delta = \rho_t/\rho_j$$

U being the penetration velocity, V the jet velocity, P the depth of penetration, and L the length of the jet (considered to be of uniform velocity). And in the non-ideal case the equation for crater volume, equation 6, became

$$\tau = T/4\overline{\phi} \tag{13}$$

where T is the kinetic energy of the projectile just before it strikes the target.

In most of the treatments of penetration by shaped charges, except that of Eichelberger,[2] who took into account the static yield strength of the target, ϕ has been considered negligible. The study made at this laboratory pointed out that the idealized theory has given good results when one is well within the realm of type (b) penetration. This theory, however, was expected to break down in the realm of impact explosions on the high velocity side and on the other hand also when the velocity was reduced to approach the threshold of plastic deformation.

Theoretical developments of the ϕ and $\overline{\phi}$ functions were next carried out. The dynamic yield strength, ϕ , was considered to consist of four terms as follows:

$$\phi = h + g + S + \sigma \tag{14}$$

where h is the specific adiabatic work of compression on the target material, g is the permanent specific shock heating of the target material resulting from the difference in entropy between a shock compression and an adiabatic compression, S is the energy radiated from the collision zone by shock waves, and σ is the static yield strength of the target. Through application of an equation of state for metals[3] the h and g functions were evaluated to be as follows:

$$h = a\beta_o^{-1} (x^a/a - 2.3 \log x - a^{-1}) \tag{15a}$$

$$g = \overline{C}_s k (x - 1)^3/x^3 \tag{15b}$$

where β_o is the compressibility at atmospheric pressure, $x = \rho_t/\rho_{t_o}$, $\underline{a}$ is a slowly varying parameter which for most metals has values which range between 2 and 2.15, k is a constant computed to be 1.88×10^4, 1.53×10^4, 1.84×10^4 and 1.26×10^4 ^{o}K for iron, lead, copper, and aluminum, respectively, and $\overline{C}_s$ is the average heat capacity per unit volume of the target material. The density ratio before and after compression was related to the pressure through the relations

$$\beta/\beta_o = (\rho_{t_o}/\rho_t)^a \tag{16a}$$

$$p = (\beta_o/\beta^{-1})/a\beta_o \tag{16b}$$

It should be stressed here that the effective pressure used in computing the density ratio was the Bernoulli pressure of flow, $\rho_t U^2/2$.

No way of evaluating S was worked out. However, comparisons between measured and theoretical (based upon the non-idealized theory) U/V vs V curves showed that S was only important in very low velocity impact, i.e., at about the threshold for plastic deformation of the target. One would expect this result also from framing camera pictures taken of shaped charge jets penetrating transparent targets which showed that in supersonic penetration the shock wave did not propagate into the target ahead of the collision zone and thus did not radiate energy from the collision zone. This occurred only for subsonic penetration. The static yield strength, σ and h, the adiabatic work of compression, were found to be the largest contributors to ϕ. In the case of steel, for example, g is generally about 0.1 as great as h.

More exact calculations for the threshold velocity, V_{ct}, to produce target explosions were performed, V_{ct} being taken to be the velocity where the internal heating of the target by adiabatic work of compression plus shock heating equaled the heat of vaporization of the metal, i.e.,

$$h_c = (a\beta_o)^{-1} [x^a/a - 2.3 \log x - a^{-1}] + \bar{C}_s k(x-1)^3/x^3 \qquad (17)$$

Some representative results are given in Table II which may be compared with those of Table I.

Table II: Threshold conditions for impact explosions according to non-idealized theory.

Metal	h_c dynes/cm^2 x 10^{-11}	ρ_o/ρ_c	p_{ct} dynes/cm^2 x 10^{-11}	U_{ct} km/sec	V_{ct} (km/sec) (steel projectile)
Iron	5.2	0.56	23.8	6.9	14.7
Copper	4.7	0.55	21.8	6.2	13.7
Lead	1.1	0.57	5.5	2.8	6.6
Zinc	1.3	0.62	4.7	3.1	6.5
Aluminum	2.3	0.56	10.9	8.0	13.3
Magnesium	1.1	0.58	5.6	7.2	11.0

Note that as far as p_{ct} and U_{ct} are concerned, the results in Tables I and II were not exceedingly different. However, V_{ct} was significantly different.

Crater volume in ultra-high velocity impact (type c cratering) was then treated theoretically. Under this type cratering the crater was considered to be divided into two zones, a zone (a) which comprised the part of the target where vaporization or impact explosion occurred, and zone (b) which comprised the region of plastic deformation. The crater made in zone (b) was considered that which would be created by an explosive detonated in the volume V_a whose available energy was $\bar{T}_a$, where V_a and $\bar{T}_a$ were related through the expression

$$\bar{T}_a = mv^2/2 - V_a h_c = V_a \rho_t U^2_{ct}/2 \qquad (18)$$

$V_a h_c$ being the energy lost in vaporization of zone (a) of the target, and $V_a \rho_t U^2/2$ being the energy available for secondary penetration in zone (b). (Note that equation (18) neglects heat loss in the projectile.) The volume in zone (b) was then taken to be that given according to equation (13), i.e.,

$$V_b = \bar{T}_a/4\bar{\phi} \qquad (19)$$

Solving for V_a from equation (18) yielded the equation

$$V_a = mV^2/2 \ (h_c + \rho_t U_{ct}^2/2) = mV^2/2p_c \qquad (20)$$

The total crater volume was then determined to be

$$V_t = V_a + V_t = V_a (1 + \rho_t U_{ct}^2/8\bar{\phi}) \doteq V_a \rho_t U_{ct}^2/8\bar{\phi} \qquad (21)$$

The volume of zone (a) was shown to be negligible compared to that of zone (b) even when $V \gg U_{ct}$ since $\rho_t U_{ct}^2 \gg 8\bar{\phi}$.

Table III lists some representative ϕ/p vs p data for steel penetrating mild steel targets which was calculated using equation (14) (neglecting S) and equations (15a) and (15b).

Table III: Computed ϕ/p vs p data for steel penetrating mild steel targets.*

p	ϕ	ϕ/p	p	ϕ	ϕ/p
15.2 (P_{ct})	5.2	0.34	0.6	0.13	0.22
10.0	3.0	0.30	0.4	0.092	0.23
8.0	2.3	0.29	0.2	0.05	0.25
6.0	1.6	0.27	0.1	0.03	0.30
4.0	1.0	0.25	0.08	0.028	0.35
2.0	0.48	0.24	0.06	0.026	0.43
1.0	0.23	0.23	0.04	0.023	0.60
0.8	0.18	0.23	0.02	0.02	1.0

* ϕ and p expressed in dynes/cm$^2 \cdot 10^{-11}$

One will note that ϕ/p varied between the relatively narrow limits of 0.34 to 0.22 from p_{ct} to 0.04 p_{ct}. Thus, it was concluded that for type (b) cratering 30 to 40 percent of the primary impact energy, $\rho_t U^2/2$, would be lost as heat in residual flow and the rest would be lost in overcoming the yield strength, σ. On this basis $\bar{\phi}/\sigma$ was concluded to be roughly 1.4-1.7. This approximated the experimental value of $\bar{\phi}/\sigma = 1.75$ which had been determined for steel jets penetrating steel targets. Thus, it was concluded that the approximation $\bar{\phi} = 1.75\sigma$ could be used in the equation $\tau = T/4\bar{\phi}$ for the crater volume in type (b) cratering.

C. <u>Observations of Vaporization Accompanying Ultra-High Velocity Impact</u>

The results of this study were described in item #8 of the list of technical notes. Briefly, experiments were carried out at velocities up to 8.5 km/sec using shaped charge jets and explosively propelled projectiles with a variety of target and projectile materials. Initially, the impacts were recorded by microsecond

color framing camera photographs. These photographs revealed that at sufficiently high impact velocities, depending upon the target and projectile materials involved, vapors were generated at impact. These vapors were highly luminous, their luminosity being found to result primarily from the decay to lower energy states of the exited and ionized gaseous metallic species making up the vapor, rather than chemical reaction with the atmosphere surrounding the impact zone. This conclusion, which proved that the clouds were a vapor rather than fine solid particles, was based upon the fact that (1) impact generated vapors were found through probe conduction measurements to be highly conducting and therefore ionized to an appreciable extent. Consequently, the term impact-generated plasmas was applied to these luminous, impact-generated clouds. (2) The luminosity of these impact-generated clouds was longer lasting and apparently just as intense when the impact took place in as near perfect a vacuum as was possible to produce. (3) Impacts in an atmosphere such as oxygen, which should react chemically with the material of the cloud, in general, were no brighter than impacts in relatively inert atmospheres. And (4) impacts involving materials possessing low cohesive energies such as lead (which one would expect to vaporize most easily) produced more intense plasmas than materials which should be more difficult to vaporize but which would tend to react more energetically with the atmosphere.

Techniques also were applied which collected small quantities of condensed vapors, the arrangement being such that the likelihood of collecting solid particles was minimized. Such samples were analyzed quantitatively to determine the ratios of the projectile or jet to target metals in the vapor condensate as a function of impact velocity. In most cases the material collected consisted of metal oxides but the X-ray diffraction patterns did not permit conclusive identification of specific compounds. These studies showed that for all the systems investigated the metal with the lower heat of vaporization was more abundantly vaporized, a fact which agreed with the results of the photographic studies. Studies with copper and steel used alternately for the jet and the target indicated that as far as vaporization was concerned, it did not matter whether a particular metal made up the target or the jet. In all cases more copper vaporized than iron. This fact was not in agreement with the prediction that projectiles would vaporize more easily than targets. Another diagreement with the predictions of the theory described

earlier pertained to the threshold for vaporization. In practice vaporization was found to occur at lower velocities than calculated, although this was not surprising.

In instances where substitutional solid solution alloys were possible such alloys could form in the impact region. For example, a copper target was impacted by a steel jet after piercing a thin 3% zinc-aluminum alloy sheet inserted in front of the target. The surface of the copper target was shown by X-ray fluorescence to contain zinc. Furthermore, the most intense diffraction peak (111) for copper was shifted through a double Bragg angle of 0.47°. The peak was less sharp than for pure copper and was also asymmetric indicating that the lattice expansion was not uniform throughout. Nevertheless, if as a first approximation the location of the peak maximum was assumed to represent the average lattice, an average lattice expansion of 0.039 Å was obtained which is equivalent to a substitution of 6% zinc in the copper lattice near the surface. Thus, simultaneous condensation of zinc and copper vapor on the surface of the copper target resulted in the formation of brass.

It was concluded that a more reliable method of sampling the species from the impact generated plasmas was required before the mechanism governing the vaporization under hypervelocity impact could be determined experimentally. However, the study did serve to show that significant amounts of vaporization did occur under proper conditions.

D. Mechanism for Crater Expansion in Shaped Charge Penetration

The results of this study were given in item #9 of the list of technical notes. This study consisted firstly of extending the model developed in item #3 of the list of technical notes which predicted final crater diameters resulting from the penetration of solids by shaped charge jets, the extension being the development of an equation which predicted the radius of the crater as a function of depth during the process of formation, namely

$$r^2 = 2r_o 1 + r_o^2 \tag{22}$$

where r is the crater radius at depth, 1, and r_o is the radius of the jet. Secondly, final crater diameters in metals penetrated by shaped charge jets comprised of various materials were compared with predictions of final crater diameter from the theory for final crater diameter. Thirdly, the shapes of craters during formation in transparent solids and liquids as photographed by means of microsecond framing camera techniques were compared with predictions of the dynamic theory.

Tables IV, V and VI present respectively comparisons of measured final crater diameters with computed values for steel, copper, and aluminum jets penetrating targets composed of various metals, d_o referring to the jet diameter, d' the computed final crater diameter, and $d(exp)$ the average measured final crater diameter.

Table IV: Comparison of computed and average measured hole diameters for steel jets

Jet striking velocity (km/sec)

Target	5.1 km/sec(d_o= 1.86 mm)		7 km/sec(d_o= 1.85 mm)		8.5 km/sec(d_o= 1.87 mm)	
	d' (mm)	$d(exp)$ (mm)	d' (mm)	$d(exp)$ (mm)	d' (mm)	$d(exp)$ (mm)
Lead	85	55	119	68	144	76
Copper	20	21	27	27	34	32
Aluminum	21	17	29	29	35	32
Zinc	13	17	18		22	28
Fe	13	13	18	16	22	21

Table V: Comparison of computed and average measured final hole diameters for copper jets.

Jet striking velocity (km/sec)

Target	5 km/sec(d_o= 0.99 mm)		8.0 km/sec(d_o= 0.93 mm)		8.6 km/sec(d_o = 1.61 mm)	
	d' (mm)	$d(exp)$ (mm)	d' (mm)	$d(exp)$ (mm)	d' (mm)	$d(exp)$ (mm)
Lead	47	52	67	68	128	73
Steel	7	9	11	15	20	20
Aluminum	8	15	11	33	22	45
Zinc	7	12	10		19	29
Cu	11	11	16	16	31	31

Table VI: Comparison of computed and average measured final hole diameters for aluminum jets.

Jet striking velocity (km/sec)

Target	5.4 km/sec(d_o= 2.2 mm)		8.8 km/sec(d_o= 1.78 mm)		9.8 km/sec(d_o= 1.88 mm)	
	d' (mm)	$d(exp)$ (mm)	d' (mm)	$d(exp)$ (mm)	d' (mm)	$d(exp)$ (mm)
Lead	77	62	101	83	119	103
Copper	19	21	25	29	29	27
Aluminum	21	21	28	28	33	33
Zinc	10	22	13		15	41
Steel	10	13	13	25	15	39

In equation (3), which was used to compute the final crater diameter, d_o was unknown. Although from flash radiographs and high speed photographs in vacuum obtained at this laboratory the jet diameter d_o was known to be of the order of magnitude of a millimeter for the particular shaped charge liners used, the actual value of the jet diameter was estimated by applying equation (3) to the measured final hole diameters in targets of the same metal as the jet (d_o in this case being the only unknown). This estimated value of the jet diameter was subsequently used in equation (3) to compute the final crater diameters in the disimilar metals. The comparisons between measured crater diameter and computed diameters were considered to be reasonably good in view of the fact there was considerable uncertainty in the values of the compressive yield strengths involved. For example, in the case of lead values of ultimate tensile strength (which was used in lieu of compressive yield strength since the two are supposed to be comparable and no compressive yield strength data were available) have been quoted which vary from 1600 lb/in^2 to as high as 3300 lb/in^2. In the calculations 2000 lb/in^2 was used because it was considered to be most appropriate to the type metal used in the targets. However, had 3000 lb/in^2 been used the agreement in general would have been much better. Table VII lists the compressive yield strengths used in the calculations. Where compressive yield strength data were not available the ultimate tensile strength was used because the two values are generally comparable.

Table VII: Compressive yield or ultimate tensile strengths*

Material	(lb/in^2)	($dyne/cm^2$)
Lead (cast)	2,000	1.4×10^8
Steel (1018, hot rolled)	70,000	5×10^9
Copper	32,000	2.3×10^9
Aluminum (1100-H-12)	15,000	1.05×10^9
Zinc alloy (96% Zn, 4% Al)	40,000 shear	4.2×10^9
	60,000 Comp	

*From ASM Metals Handbook.

The formation of craters in transparent targets by shaped charge jets was investigated by backlighting the target with an explosive lightbomb and photographing the penetration of the jet and the expansion of the crater with a high speed framing camera. The transparent substances studied were: water ($\rho = 1.0$); acetylene tetrabromide ($\rho = 2.96$); saturated aqueous zinc chloride solution ($\rho = 1.88$); gasoline ($\rho = 0.79$); lucite ($\rho = 1.18$); carbon tetrachloride ($\rho = 1.59$); and chloroform ($\rho = 1.49$). The jet velocities used were 5.1 km/sec, 7.0 km/sec, and 8.5 km/sec, the jets in all cases being steel and originating from liners identical with those used in the final crater diameter studies in metals. Consequently, the previously determined jet diameters were available for use.

From the framing camera sequences the instantaneous extent of forward penetration was plotted against the instantaneous hole radius and the results compared to equation (22). The experimental data were found in general to fall quite well along the theoretical parabolic curve. No trend away from the theoretical curve was discernable for gasoline and water or lucite and chloroform which possess comparable densities. However, in the case of carbon tetrachloride, zinc chloride solution, and acetylene tetrabromide, each representing a material of increased density, there was an increasing tendency for the crater diameter to exceed theoretical values. Moreover, this tendency became more pronounced at higher velocities. At the writing of AFOSR-TN-60-851, no explanation was advanced to explain why the ratio of the lateral expansion velocity to the forward penetration velocity increased with target density and jet velocity. However, since that time the thought has been advanced that the effect could be due to increased compression of the target material between the crater and the shock front resulting from higher pressure generated by increasing the density of the target material or the jet velocity.

E.   Ionization and Electron Densities in Detonation Solid Explosives

The results of this investigation were described in item #1 of the list of technical notes. This important investigation formed a basis for some of the theories of detonation and external detonation-generated plasmas advanced later by this group. Some of the results obtained in this study were corroborated by papers given four years later at the Third ONR Symposium on Detonation, Princeton, New Jersey. These experiments involved consisted of determining the specific

electrical conductivities within detonation waves of solid explosives and mapping out the shapes of the conducting regions. Both of these determinations were made through the application of conduction probe techniques. By means of a theoretical expression for mobility of electrons under the conditions prevailing in detonation waves and the measured conductivities the electron densities were calculated. The resulting values which ranged from $0.2 \times 10^{17}/cm^3$ for low density granular 80/20 AN/TNT mixtures to 6×10^{17} $1/cm^3$ for Composition B were believed to represent underestimates of the actual electron densities.

Considerations were given as to mechanism through which such high electron densities could be created. Thermal ionization, for example, had to be eliminated because under the exceedingly high pressure, relatively low temperature conditions involved in detonation waves the process of thermal ionization would lead to electron densities orders of magnitude lower than was measured. More or less through a process of elimination the conclusion was finally reached that the electrons were a result of chemionization which occurred during the extremely rapid chemical reactions involved in detonations. In the light of this conclusion electron-ion re-combination times in the detonation wave were considered. Kinetic theory approaches were applied to the problem with the result that average re-combination times were calculated to be about 10^{-12} seconds for electron positive ion recombination and they would, of course, be shorter in the case of negative ion formation. Such recombination times were considered to be unrealistically short, however, because electron transition times were known to be the order of 10^{-8} seconds. On this basis it was concluded that electron lifetimes in detonating explosives were limited not by purely kinetic effects but by recombination probabilities and that the lifetime was probably the order of 10^{-8} seconds.

Since chemical reaction times in detonation were known to be the order of microseconds or roughly one-hundred times the expected lifetime of an electron, it was concluded that electrons would be measured only in regions where they were being formed. Thus, the conduction zone in detonation waves corresponded to the chemical reaction zone. On the basis of the high electron densities and their short lifetimes it was also concluded that at some stage during the reaction each molecule of explosive contributes a free electron and possibly an electron is freed wherever a chemical bond was broken.

Measurements of the length of the conduction zone were then compared to
chemical reaction zone lengths which were determined from detonation velocity vs
diameter curves by the existing theories, namely the Eyring "curved front" theory,[4]
the Jones "nozzle" theory,[5] and the "detonation head" model of Cook.[6] These
comparisons revealed that in every case where the explosive was ideal (the deto-
nation velocity equaled the "leveled off" or hydrodynamic value) the length of the
conduction zone at the charge axis equaled within a factor of two the reaction
zone length given by the detonation head model, and generally the agreement was
closer than this. Table VIII is a reproduction of a table given in the original
report showing these comparisons. In the case of the two non-ideal explosives,
coarse TNT and 80/20 AN/TNT, the conduction zone lengths were much shorter than
the reaction zone lengths determined by the "detonation head" model.

The shapes of the conduction zones mapped out by the probe technique were
then compared with the "detonation head" model. In unconfined cylindrical charges,
according to the premises of this model, a high density, high pressure region
(called the detonation head) with approximately uniform density prevails in the
detonation wave. When the detonation wave is steady state and fully formed, this
high density region is the shape of a cone whose base coincides with the detonation
wave front and whose sides are bounded by lateral rarefaction or release waves
which propagate into the charge starting at the detonation wave front. The length
of the detonation head is said to equal approximately its diameter which in turn
equals the diameter of the charge minus a small edge effect of about 0.6 cm.
According to this model the detonation wave propagates at a velocity determined
by the extent of chemical reaction occurring along the streamline of maximum
length inside the detonation head. Thus, explosives with a reaction zone length
a_o equal to or less than h, the length of the detonation head, are ideal, and
those with longer reaction zone lengths are non-ideal. For reaction zone lengths
which were shorter than the length of the detonation head, the ionized zones as
determined by direct mapping with the probes were found to have approximately the
shape of truncated cones, the length of the zone becoming less toward the surface
of the charge. The rear surface of the zone as already stated corresponded
roughly to the end of the reaction zone predicted by the detonation head model and
the sides of the zone apparently were defined by the inward moving lateral rare-
faction waves previously mentioned that define the detonation head. This is not

Table VIII: Comparisons of reaction zone lengths a_0 from current theories with steady state ionized zone lengths determined with probes in 5.08 cm diameter charges.

Explosive	Density (gm/cm)	Particle Size (cm)	Nozzle Theory a_0(cm)	τ(μsec)	Curved Front Theory a_0(cm)	τ(μsec)	Detonation Head a_0(cm)	τ(μsec)	Average conduction zone length at charge axis (cm)
PETN*	0.91	0.0357	0.11	0.21	0.05	0.093	1.1	2.1	2.0
RDX*	1.00	0.052	0.12	0.26	0.046	0.10	1.2	2.6	2.1
Tetryl*	1.00	0.071	0.20	0.54	0.08	0.216	2.0	5.4	2.3
EDNA*	0.98	0.0357	0.35	0.6	0.2	0.35	3.5	6.0	2.8
Fine TNT*	0.90	0.0417	0.21	0.59	0.08	0.24	2.1	5.9	2.9
Coarse TNT	1.03	0.284	1.55	4.05	0.61	1.6	15.5	40.5	4.1
80/20 AN/TNT (AN particle size listed)	1.00	0.0412	2.97	9.0	1.19	3.6	29.7	90.0	2.7
Cast TNT*	i.67	No values available							2.1
Cast Comp B*	1.69	No values available							1.9

A * designates the particular explosive was ideal in 5.08 cm diameter. Other explosives were non-ideal in this diameter.

surprising on the basis of the assumption that the ionization is produced by
chemical reaction since it is clear that the temperature, and consequently the
chemical reaction rate, must drop sharply at the boundaries of the detonation
head. For non-ideal explosives it was expected that the conduction zone should
just correspond to the fully formed detonation head. In the case of coarse TNT
the length at the axis corresponded well but the off-axis lengths tended to extend
past the boundaries of the detonation head. For the 80/20 AN/TNT mixture the
conduction zone length at the charge axis was somewhat shorter than the detonation
head. This mixture, however, presented difficulties which made determinations of
the actual conduction zone length difficult. With this explosive the fine TNT in
the mixture reacted much more rapidly than the ammonium nitrate. After the TNT
reacted, the conduction corresponding to the reaction of the AN dropped to low
values which were difficult to measure.

The results of the above study explained the origin of the ionization in
external detonation generated plasmas which will be discussed later. They also
provided a foundation upon which new theories of detonation were built. For
example, the presence of such high electron densities in detonation reaction zones
with their associated high mobilities suggested that the conduction of heat within
the wave was appreciable in contrast to the classical theory of detonation which was
based upon transport phenomena in detonation waves being negligible. In fact,
there are reasons to believe that sufficient heat conduction is a necessary con-
dition for detonations to occur as will be discussed later.

F. Electrical Fields and Electromagnetic Radiation from Chemical Detonations

The results of this study were described in item #7 of the list of technical
notes. During the course of some field work carried out by this group, which
utilized the initiation of explosives by a portable 1-1/2 volt battery firing unit,
the two firing leads were accidentally touched during an explosion, and a strong
electrical shock was experienced. A further study of this phenomenon revealed that
appreciable electrical fields existed around explosions. These preliminary studies
provided motivation to investigate the types of electrical manifestations resulting
from chemical detonations and the mechanisms whereby they were generated.

Due to the fact that such a large number of varied experiments were carried out
as a part of the program it is not practical to describe them all in this final

report. Hence, only the main general conclusions will be discussed as well as a brief description of the general experimental method.

Measurements were made for charges ranging in size from 10g to approximately 25 kg over a frequency range extending from a few cycles/sec to 500 megacycles. Most of these measurements were made with the charge to pickup separation ranging from several meters to a hundred meters or so, which would lie well within the induction zone for frequencies below the megacycle range. It was expected at first that most of the signals would be above 10 kc. Hence, in first experiments a broad band system consisting of a 2 meter length whip antenna feeding directly into the pre-amplifier stage of a Tektronix 545 oscilloscope was used. Results soon showed, however, that the strongest signals were in a lower frequency range, which dictated that equipment covering a broader spectrum be used. For subsequent measurements, depending on the information desired, one or more of the following pickups were used: a 5000 megohm input impedance cathode follower with a maximum frequency response of 100 kc, a 1000 megohm input impedance cathode follower, a 1 megohm input impedance completely transistorized emitter-follower with a high frequency cut off of 1 megacycle, a 500 mc receiver, a 98 cm receiver, and a 50 mc receiver. The cathode followers were all battery operated and were designed such that their pickup antennae were maintained at ground potential, 10 cm diameter copper spheres being used for antennae. In each case the low frequency cut off was determined by the input impedance, the distance from the signal source, and the type antenna employed. A horizontal yagi antenna was used with the 500 mc receiver, while with the 98 mc and 50 mc receivers one-half wave length vertical or horizontal dipole antennae were used. In all cases recordings were made with Tektronix 545 oscilloscopes.

A 10 KV square wave calibrator was constructed to assess the linearity of response of the low frequency cathode follower systems at frequencies essentially down to 10 cps. This calibrator charged a 25 cm diameter spherical conductor with an 8 KV square wave, the signal from which was picked up by the cathode follower systems. It was found possible to achieve nearly linear D.C. response for 6m separation between the pickup and the 25 cm ball by use of a 0.01 mfd capacitor connected from the antenna to ground in the case of the 1000 megohm input impedance cathode follower system. Thus, when very low frequency response was desired such an integrating capacitor was used. A capacitance of 0.01 mfd was a

compromise value, however, as larger capacitors lead to somewhat more linear response but they decreased the gain prohibitively. The rise time of the 1000 meg-ohm input impedance cathode follower system under these circumstances was found to be about 10 μsec from which an estimate of 50 KC for the high frequency cut off was obtained.

One of the greatest difficulties encountered in carrying out the experiments was the reduction of background noise to useable levels. This noise resulted primarily from circuitry employed originally to trigger the oscilloscope and to fire the electric detonators which initiated the charges. The first problem was circumvented by employing a battery powered transistorized photocell trigger unit which triggered the oscilloscopes from the first light either of the explosion or an auxiliary flash which was timed to occur a few microseconds before the explosion. Electric detonator systems were abandoned early in the program because the presence of wires near the explosion was found to alter the signals considerably. Experience also proved that any obstructions near the charge exerted an influence on the signals. Hence, in most tests the charges were suspended above the ground, away from any obstructions, by a nylon string. In order that the charge be as free as possible from external influences at the time of detonation a special method of initiation was employed. An ordinary fuse blasting cap was used to initiate the charge, the fuse being ignited electrically by a squib. As near to the blasting cap as possible (about 1") the fuse was cut and a section of JPN propellant was inserted which upon "burning through" allowed the burned fuse to separate and the section connected to the squib and the squib lead wires to fall to the ground. Thus, before the explosion occurred the charge hung perfectly free.

The more important experimental results that were obtained may be summarized briefly as follows:

(1) The largest voltages generated by chemical detonations were found to lie in a frequency range below a few hundred cycles/second. Only a small fraction of the low frequency signals was radiated.

(2) The dominant frequency, provided the explosive was free from obstructions, was found to decrease with charge size. Also, the electrical potential generated by an explosion was found to increase with charge size. Accurate absolute evaluations appeared to be impossible because the geometry and charge distribution of the signal

source created by the explosion was not accurately known. However, in magnitude the potential appeared to increase in direct proportion to charge weight. By means of direct calibrations of equipment and assuming that the signal source was equivalent to an expanding charged sphere whose diameter equaled the diameter of the detonation products, -18,000 V was determined to be the maximum signal source potential for a 552g pentolite charge.

(3) Accurate determinations of attenuation with distance of the detonation generated electrical fields were difficult because the frequency response of the equipment varied with the charge to pickup distance.

(4) As a rule initially the electrical potential of the detonation-generated signal source became uniformly more negative with time until a maximum was reached. Thus, as charge was lost, its potential became less negative. In most instances the signal source potential remained negative with respect to the earth for the duration of the signal. Intermediate frequencies seemed to be generated largely by the expanding cloud of detonation products hitting obstructions or contacting grounded conductors.

(5) The reproducibility of the detonation-generated electrical fields was markedly affected by obstructions, principally grounded conductors (even though they possessed high impedances) which were contacted by the expanding detonation products. Another even more important factor was the blowing of dust from the earth's surface by the explosion. Enclosing the charge by a layer of plaster of paris, for example, markedly increased the signals at all frequencies. The low frequency component could be enhanced by a factor as high as 20 by this process.

(6) Increased outputs from cathode followers covering both a low frequency range and an intermediate frequency range were observed when the charge height was increased within certain limits. Such increases did not result from an increased potential of the detonation-generated signal source but rather from decreased distortion of the electrical field by the earth as the height was increased. This fact was borne out by static calibrations in the laboratory.

(7) No significant effects of charge shape, charge orientation or position of the detonator on the charge were observed on low frequency and intermediate frequency electrical fields. The effect upon the high frequencies in this regard was not determined.

(8) Experiments were carried out in a RF cage which was sufficiently large to contain both the explosion and the pickup antennae. Means were available to control over a wide range the static electrical field within the cage. Results showed that the static electrical field surrounding an explosion had little effect upon explosion-generated electrical fields or the EM radiation.

(9) The high frequency radiated energy occurred in the form of short, random bursts which covered a broad band of frequencies. In many cases some of the bursts of radiation were observed to correspond to higher frequency transients manifested on oscillograph traces of the outputs from low frequency response cathode followers.

(10) The detonation-generated radiation bore a strong resemblance to radiation resulting from corona discharge.

(11) With bare charges there was found to be a non-reproducible delay between initiation and the first bursts of radiation. This delay was generally at least several hundred microseconds and could be as much as several milliseconds. When charges were enclosed by a layer of plaster of paris this delay was reduced.

(12) Increasing the charge size increased primarily the number of bursts of radiation rather than their amplitude.

(13) Most of the radiation pulses contained both vertical and horizontal electric field components, although cases were observed where the bursts were completely vertically or horizontally polarized.

(14) During the later stages of the expansion process, when the explosion was sufficiently close to the earth, the vertical component of the radiation was found to predominate and was markedly enhanced at the instant of impact of the gas cloud with the ground.

On the basis of the above results a mechanism was proposed as follows: The results cited concerning the large enhancement of signal when the charges were enclosed by inert solids show that the air shock generated by the blast or the external explosive plasma are unimportant as sources of electrical signals because a layer of the inert material eliminates the plasma and attenuates the air shock considerably. The enhancement of the low frequency signals produced by inert, solid confinement can be visualized to occur in the following way: The force of the explosion accelerates to high velocities the small particles formed when the solid is pulverized. These small, high velocity particles pick up an electrokinetic

charge as they move through the atmosphere thus forming an expanding cloud of charged particles. By virtue of the fact that these inert particles pick up more and more charge as time goes on and at the same time the expanding cloud grows larger and larger, the electrical field sensed by the pickup increases. The length of time that the electrical field continues to grow, as well as its magnitude, would therefore be expected to increase with charge size. This external field finally decays to zero when the velocity of the particles become so low that they lose their charge. Contact of the expanding cloud with the ground will increase the rate at which it loses its charge as shown by charge height studies. Contact with the ground, other conductors and probably also even other rather massive nonconductors can introduce transients in this external field. These transients, however, may or may not be abrupt enough to generate megacycle components which may be measured as radiation. In fact, the electrokinetic effect of small, high velocity, solid particles may also account for the observed electrical effects even for bare charges. All explosives exhibit an "edge effect." That is, a small layer of explosive around the charge is not immediately consumed by the detonation in unconfined charges. Possibly some of this material may be propelled outward in the form of high velocity microparticles. However, this explanation for bare charges is not justified from the evidence yet available.

As mentioned above, transients in the external field can be produced in various ways. It is felt that the high frequency components (i.e., 50 MC, 98 MC and 500 MC) may be generated primarily by miniature "lightning bolts" occurring between regions of differing potential within the signal source. This suggestion seems to be borne out by the observed delays between the detonation and the first bursts of radiation as well as the randomness of the bursts and their resemblance to radiation generated by corona discharge. This model to account for high frequencies also seems to agree with the effect of charge size. That is, there appears under a given set of conditions, to be a minimum charge size which will generate frequencies in the megacycle range. As charge size is increased, the most striking effect produced is that the radiation pulses occur much more frequently with only a small increase in magnitude. This suggests that a critical value of potential gradient must exist within the expanding cloud in order for a pulse to be generated.

It has been noted that when charge sizes around 100g are used no 50 MC or 98 MC signals are detected, while at other times using the same sensitivity settings signals will be received. This suggests that some properties of the surrounding gaseous medium subject to change may determine whether or not critical conditions may attain within the signal source cloud. One possible factor is humidity. However, no attempts have so far been made to evaluate this factor.

G. External Detonation-Generated Plasmas

The results regarding this subject have been described in items #5, #10 and #12 of the list of technical notes.

When the detonation wave front reaches a free surface of a charge in air, for example the end of a cylindrical charge, a highly luminous cloud is formed which propagates away from the charge at high velocity. This phenomenon had been observed by others as well as members of this group for a long time but had attracted little interest because the luminosity was thought to be simply a result of thermal ionization in a shock wave generated in the atmosphere surrounding the charge. While studying microsecond framing camera photographs in color showing detonations of liquid explosives, it was noted that the luminous cloud which appeared at the free surface of the liquid exhibited a remarkable tendency to "hang together" as it propagated through the atmosphere. The interest kindled by this observation led to further investigations of the phenomenon which were carried out under this contract.

Through probe conduction techniques, these luminous clouds, as expected, were found to be highly ionized. The electron densities, in fact, were estimated to be the order of 10^{16} $1/cm^3$ or about 1/10 to 1/100 the density prevailing in detonation reaction zones. The first concern naturally was determining the origin of this ionization. Thus, the mechanisms which could possibly be effective were formulated and considered. These mechanisms were:

(1) Unreacted or partially reacted explosive is spalled from the end of the charge upon the arrival of the detonation wave. This material reacts as it is propelled from the charge and by virtue of this chemical reaction forms ionized species.

(2) The luminous cloud consists largely of ions and electrons propelled from the detonation reaction zone. As a result of chemical reaction occurring at the surface of the explosive when the detonation wave emerges, ions and electrons

which are formed are propelled forward into a much lower density region, the expected lifetime of an electron therefore being much longer by virtue of the reduced density of gas molecules.

(3) Thermal ionization within a shock wave that is generated in the gaseous medium outside the charge upon the emergence of the detonation wave.

Mechanisms (1) and (3) were soon discounted by early experiments, and this conclusion was later verified by a large number of facts gained through subsequent research. Early experiments, for example, were performed in which the ionization generated by pure shock waves was compared to that produced when a detonation wave emerged from the end of a bare charge. Among these comparisons possibly the most striking was that obtained using a charge comprised of a 92/8 mixture of fine explosive grade ammonium nitrate-nitropropane whose end was bare and a 2"dia x 8" length Composition B charge whose end was terminated with a 1/4" thick glass plate, glass incidentally being a fairly good impedance match for Composition B. In the case of the glass-terminated Composition B charge no luminosity was apparent on a framing camera sequence of the event. However, a luminous cloud propagated from the free-ended ammonium nitrate-nitropropane charge (which was photographed simultaneously with the Composition B detonation) when the detonation wave reached the free end. Calculations revealed that the pressure of the shock wave driven by the glass-terminated Composition B charge was at least as great as the pressure of a shock wave which could be driven by the bare-ended AN-NP charge. Such detonation-generated luminous clouds, in fact, have been observed to propagate from free surfaces of charges no matter how weak the detonation is as long as it occurs. Respectable luminous clouds, for example, have been observed to be generated by detonations in 94/6 ammonium nitrate-fuel oil mixtures where the detonation pressure was as low as 13 kb.

As mentioned earlier, framing camera sequences obtained of detonation liquid explosives in glass beakers showed that the luminous cloud generated at the surface of the liquid did not expand significantly as it left the top of the beaker, which is not the behavior one would expect from a shock wave. Furthermore, the cloud did not exert sufficient external pressure to fracture the beaker before the deto-nation products following somewhat behind shattered it. Experiments with conduction probes revealed an interesting pulsating phenomenon. Under certain conditions the length of the luminous cloud was observed to oscillate and the conduction varied with

the oscillations, being the greatest when the plasma length was the shortest and the least when it was the longest.
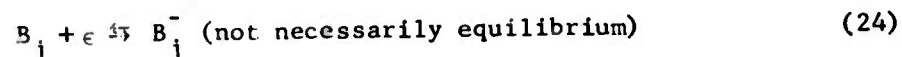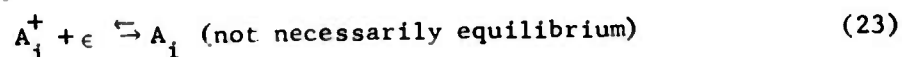
On the basis primarily of the aforementioned evidence, mechanism (2) was considered the most applicable, and the luminous ionized clouds were termed "external detonation-generated plasmas" in contrast to the ionization in the detonation reaction zone which was termed the "internal detonation-generated plasma". Since such high electron and ion densities were known to exist in detonation reaction zones, it was not surprising that some evidence of this would be manifested exterior to the charge when the detonation wave emerged. (Considerable evidence to support this conclusion was obtained during subsequent studies, the more important points will be given below.) In order to account for the remarking cohesive properties of the external detonation-generated plasmas the "quasi-lattice" or "metallic model" for the plasma was advanced. According to this model the electrons circulate through the positive ion lattice in correlated patterns similarly as occurs in metals. In other words, the external detonation-generated plasmas were considered to involve the formation of the outermost valence electrons from localized states in atoms or molecules to collective electron states in which they moved freely, but at an appreciable negative potential energy throughout the plasma to give it appreciable cohesion. The existence of a quasi-lattice state in external detonation-generated plasmas inferred the existence of a similar state for the internal detonation-generated plasmas, or, in other words, that the detonation state was a "plasma" state. Such a structure would explain the exceedingly high electron densities in detonation reaction zones because the electrons would not be completely free but would still be bound by the cohesive energy of the lattice, and therefore the state would be easier to achieve than a completely free electron state. According to the quasi-lattice model of the plasmas, the greater the electron density, the greater is the negative potential energy of the system and correspondingly the greater is the cohesion of the plasma. However, the quasi-lattice is opposed by thermal energy. As long as the conditions prevail that $E_c \gg kT$ (E_c being the cohesive energy), then the plasma will be stable, but when E_c decreases to approach kT then the plasma will decay to an ordinary gaseous state.

On the basis of mechanism (2) the initial length of the external detonation-generated plasma, before the plasma has time to expand significantly, should be

proportional to the reaction time of the explosive, i.e., $L_p^* = kV^*\tau$ where L_p^* is the initial plasma length, k is a proportionality constant, V^* is the initial plasma velocity, and τ is the reaction time. Measurements made with nitromethane, Dithekite 13 and tetryl revealed that such was indeed the case with k equaling approximately 0.5. Further, measurements with loose tetryl of varying particle size revealed that the initial external detonation-generated plasma length was directly proportional to the particle size as is the reaction time.

Subsequent work yielded a great deal of information concerning such things as the origin, structure, decay characteristics, etc., of external detonation-generated plasmas. The more significant findings are summarized briefly below:

(1) The decay of electrons in both internal and external plasmas takes place primarily by the formation of negative ions with subsequent neutralization of the negative ions and positive ions. However, some direct positive ion capture of electrons would be expected to occur. These decay reactions are represented by the following equations:

$$A_i^+ + \epsilon \leftrightarrows A_i \quad \text{(not necessarily equilibrium)} \tag{23}$$

$$B_j + \epsilon \leftrightarrows B_j^- \quad \text{(not necessarily equilibrium)} \tag{24}$$

$$B_j^- + A_i^+ \to \text{neutral products} \tag{25}$$

The importance of negative ion formation in the decay of plasmas was illustrated by decay measurements performed for plasmas propagated into various gaseous atmospheres, the most rapid decay being observed for gases which possessed the highest electron affinities. This result showed also that the gas through which the plasma was propagated was an important contributor to the reduction of the electron density in the plasma and its subsequent decay to a gas. The electrical conductivities, measured for plasmas propagated into various atmospheres, were extrapolated to the charge surface with the result that the initial conductivities possessed the same values, indicating again that the major share of the ionization originated from the explosive rather than being generated in the gas surrounding the charge.

(2) The conduction zone of the external plasma corresponds precisely to its luminosity zone. This supports the concept that the luminosity is a result of quantum transitions and conduction is proportional to the concentration of free electrons.

(3) External detonation-generated plasmas are actually relatively high in density and therefore propagate with a relatively large amount of material in them. This fact was illustrated by framing camera pictures showing the decay and "explosions" of plasmas to a gas. The volume of gas produced as a result of such explosions has been estimated to be as much as 100 times the original plasma volume. The decay from the plasma state to the gaseous state apparently occurs when the cohesive energy of the plasma as a result of loss of electrons drops to a value approximating the thermal energy. One would expect that plasmas with high electron densities such as produced by fast reacting, high density, high velocity explosives would be more stable than those from "slower explosives, and this has proven to be the case. The decay or explosion of plasmas to a gas is promoted by interactions which tend to "stir" the plasma and weaken its lattice structure such as rapidly compressing a plasma and then allowing it to expand or impacting a barrier.

Under proper lighting conditions a non-luminous shock wave may be observed to separate from the plasma when it explodes. The interpretation of this phenomenon is that when the electron density in the plasma has dropped sufficiently that the plasma state decays to the gaseous state, the ensuing rapid expansion of the gas drives a shock ahead of it.

(4) External plasmas may decay in one gas and later reappear in another, e.g., they have been shown to disappear in propane and reappear in air. This result may be explained on the basis that the B_j^- ion decay is small via equation (25) but the reactions of the type $B_j^- + C_j \rightarrow C_j^- + B_j$ are fast. Now B_j^- ions from propane do not ionize rapidly and therefore serve as traps for electrons. However, the C_j^- do ionize rapidly. Therefore, as soon as the propane medium becomes diluted with air the free electrons reappear.

(5) Plasmas are readily manipulated by mechanical means. They can be compressed from large diameters into much smaller diameter glass tubes. They can also be readily "piped" around corners. In such experiments the cracking of the glass tubing was not sufficient to prevent transparency until a microsecond or so after the plasma had gone by.

(6) Manipulations with magnetic fields, though attempted, have not as yet proved successful presumably because of insufficient magnetic field intensity.

(7) Framing camera sequences of softly backlighted plasmas from Dithekite-13, which is oxygen balanced and possesses nearly transparent detonation products, have shown some very interesting structural features of external detonation-generated plasmas; a diagram of one picture from a sequence is given in Fig. 2. The sequence clearly showed a complicated multiple shock pattern which one would not conceive of existing were the plasma merely shock induced ionization, because under this circumstance only a strong shock at the plasma front would exist. The resulting shock pattern generated in the lucite witness block by impact of the plasma showed, however, that the shock corresponding to the front of the plasma was weak in comparison to the shock at the rear of the plasma. As already described during their existence of several hundred microseconds or so, if undisturbed in flight, external detonation-generated plasmas undergo accelerating decay which sometimes reaches explosive magnitudes. Decay occurs most rapidly in regions of low electron density and the decay promotes further decay. Since the electron densities are highest at the front of the plasma and lowest at the rear (as determined by probe measurements) the decay occurs most rapidly at the rear. Even though the density of a plasma

backlighted
lucite block

jet from plasma

plasma bow wave

recombination
shock of plasma

bow wave corre-
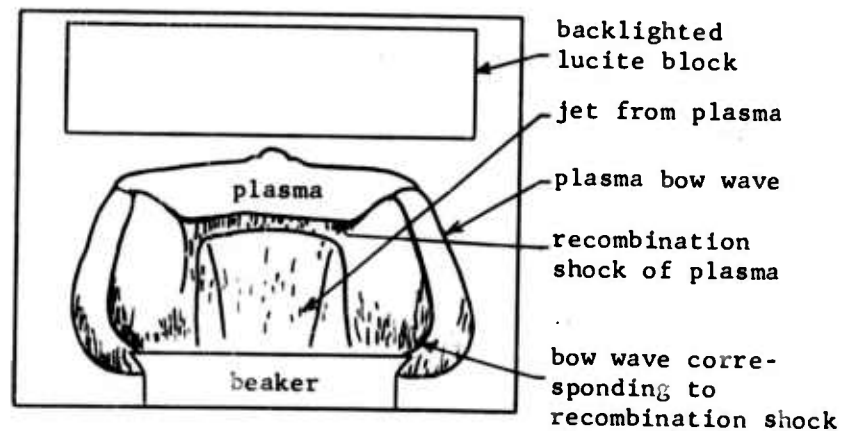sponding to
recombination shock

Figure 2. Diagram of one picture from a framing camera sequence of a "softly" backlighted plasma from dithekite 13.

may be several hundred times that of air the external detonation-generated plasmas exhibit little external pressure owing to their high cohesion. When, however, decay of the plasma to a gas occurs, the pressure rises sharply. Therefore, at the rear of the plasma where decay is occurring rapidly, a rapid pressure rise should occur. The decay and sudden rise of pressure at the rear of the plasma is believed to be the cause of the strong shock at the rear of the plasma. For this reason this shock was designated the re-combination shock. The weak shock at the plasma front, on the other hand, was considered to be simply a compressional bow wave produced by the plasma propagating through the atmosphere. According to this model external detonation-generated plasmas would be "jet propelled" by decay of the plasma at the rear to a gas. Indeed, the jetting of gases off the back of the plasma was suggested in the framing camera sequence from which Fig. 2 was taken, what appeared to be a Mach diamond being clearly evident. It is perhaps this jet propulsion in external detonation-generated plasmas that causes them to separate from the main detonation products and propagate generally at super detonation speeds. Admittedly, the above explanation departs widely from classical theory. However, there is no way evident to us whereby the classical theory of thermal ionization in a shock wave can explain the complicated shock patterns shown in Fig. 2. These patterns we feel are a justification for the model of the plasma which has been proposed.

(8) When external detonation-generated plasmas were compressed the conductivity was found to increase in a manner comparable to that in metals under compression.

(9) A more extensive study involving plasmas propagated into a wide variety of gases was carried out, the list of which included argon, air, nitrogen, oxygen, carbon monoxide, carbon dioxide, ammonia, chlorine, propane, helium, and hydrogen, all under atmospheric pressure and in addition hydrogen and air at about 0.5 mm pressure. These studies in agreement with the less extensive earlier work involving plasmas propagated into a number of gases showed that magnitude of the conductivity extrapolated to the charge surface was essentially independent of the gas, and the decay rate of the plasma was strongly dependent upon the gas as was the velocity of the plasma. In addition, it was found that the plasma could be luminous, transparent, or dark depending upon the gaseous medium and its pressure, as shown by the results given in Table IX. Measurements of conductivity therefore were concluded to be the only reliable means of determining whether or not a plasma existed. It was interesting to note that even in the case of a vacuum ionized clouds (plasmas) were propelled from

Table IX: Qualitative comparisons of visible light intensity for ionization waves propagated through various gases at ambient pressure.

Explosive	Gaseous atmosphere	Ionization potential (e.v.)	Visible luminosity
D-13*	Argon	15.7	Extremely brilliant
D-13	Air	--	Bright
	Nitrogen	15.5	Bright
	Oxygen	12.5	Bright
	Carbon monoxide	14.1	Bright
	Carbon dioxide	14.5	Bright
D-13	Ammonia	11.2	Moderately bright
	Chlorine	13.2	Moderately bright
D-13	Propane	--	Nonluminous-dark cloud forms
D-13	Helium	24.5	No detectable luminosity transparent cloud only
	Hydrogen	15.6	Same as in He
Composition B and tetryl	Helium	24.5	Weak momentary light at charge surface. No luminosity at long distances from charge
Composition B	Air vacuum	--	Very low to no luminosity depending on actual pressure

* D-13 = 63/24/13 HNO_3/nitrobenzene/water

free surfaces of detonating explosives. Experimental measurements were compared to calculations of electron density based upon hydrodynamic theory and the mechanism of thermal ionization in shock waves which were assumed to be traveling at the experimentally determined plasma velocities. These comparisons were carried out for both air and hydrogen at initial pressures of 645 mm Hg and 0.5 mm Hg. In order to minimize ambiguities that might result from the use of an incorrect probe calibration factor required to transform conductance data to conductivity data,

ratios of the conductivities at 645 mm Hg and 0.5 mm Hg were also compared. In the case of air near the surface of a bare Composition B charge $\sigma^*_{645} = 0.012$ mho/cm and $\sigma^*_{0.5} = 0.006$ mho cm were measured while $\sigma_{645} = 29$ and $\sigma_{0.05} = 130$ mho/cm were calculated giving $\sigma^*_{645}/\sigma^*_{0.05} = 2$ and $\sigma_{645}/\sigma_{0.5} = 0.2$. When the plasma was extruded into a 3/8" diameter plastic tube, the results were $\sigma^*_{645} = 0.52$ mho/cm, $\sigma^*_{0.5} = 0.26$ mho/cm, $\sigma_{645} = 130$ mho/cm and $\sigma_{0.5} = 160$ mho/cm giving the ratios $\sigma^*_{645}/\sigma^*_{0.5} = 2.0$ and $\sigma_{645}/\sigma_{0.5} = 0.8$. Thus, for air the disagreement was not sufficient to be conclusive. However, for plasmas propagated into hydrogen the disagreement between the measured conductivities and the calculated conductivities was very striking. In the case of plasmas extruded into a 3/8" diamter tube the results were $\sigma^*_{645} = 0.13$ mho/cm, $\sigma^*_{0.5} = 0.20$ mho/cm, $\sigma_{645} = 9.25 \times 10^{-6}$ mho/cm, and $\sigma_{0.05} = 0.11 \times 10^{-6}$ mho/cm giving $\sigma^*_{645}/\sigma^*_{0.05} = 0.6$ and $\sigma_{645}/\sigma_{0.5} = 82$.

(10) Pressure measurements were made with the aquarium technique by compressing plasmas into plastic tubes and allowing them to impact water. The velocities of the transmitted waves in water, by means of a suitable calibration curve, yielded the pressure. Measured pressures of plasmas were found in this manner to exceed by about a factor of 5 the pressure associated with a shock wave considered to be traveling at the velocity of the plasma. By themselves comparison of observed and computed pressure probably should not be considered sufficient to rule out the possibility of a shock mechanism. However, evidence was obtained which indicates that the actual shock wave velocity for a true shock wave was less than half the velocity of ionization waves. Hence, the actual or true value of the shock wave pressure would be only about 1/4 as great as the value computed by assuming the shock wave velocity to be the same as the ionization wave. On this basis the measured ionization wave pressures were 10 to 20 times greater than the pressure of true shock waves transmitted from the explosives into the gaseous medium. The velocity of the observed luminous wave transmitted from Composition B directly into air at atmospheric pressure was measured to be 8.3 km/sec. However, when an aluminum plate, thin enough so that there was no appreciable attenuation as determined by actual pressure measurements by the aquarium method, was placed on the end of the charge the shock wave was observed to travel at only 4.4 km/sec. Of significance is the fact that the impedance mismatch equation was found to predict quite accurately the shock pressure in gaseous media of such aluminum terminated charges (even though the equation was heretofore not been considered applicable for such large differences in impedance). Since the shock impedance

of aluminum is nearly equal to that of Composition B, the impedance mismatch equation would predict very nearly the same shock pressure in the gas for bare charges as for the thin plate aluminum terminated charges.

The shapes of the conduction traces measured for pure shock waves were different than those for ionization waves from bare charges, the latter exhibiting a more gradual rise at the front.

(11) Even though the ionization waves from hydrogen and helium were non-luminous they always generated high luminosity upon impacting the end of the glass or plastic chamber. In the case of plasmas from Dithekite-13 (since it is oxygen balanced its detonation products were transparent) close observation of the ionization waves in hydrogen and helium revealed a diffuse, non-luminous zone at the front of the detonation products that corresponded to the luminous zone in air, for example. This fuzzy zone was believed not to be due to a shock wave alone since it was too wide to be attributed to possible camera "smear" effects and it did not exhibit the change in index of refraction associated with a shock wave. The fact that the fuzzy zone was conducting was easily determined by propagating it between two plates charged to a potential difference of 20 KV which resulted in an arc discharge through the fuzzy zone.

It was concluded finally that the plasma was a precursor ionization wave generated primarily from chemionization in the detonation reaction zone which is ejected into the atmosphere and trapped in a lower density state when the electron-ion recombination times are longer. However, in the case of argon or air, for example, the thermal ionization may be considerable. The ionized material is then propagated ahead of the normal shock where it reacts with the gaseous medium to produce high luminosity in many cases. It is not unexpected that electrons and perhaps low mass ions would be radiated ahead of a shock owing to its high thermal gradient.

The luminosity is caused by the interaction of electrons in the plasma primarily with molecules of the gaseous medium (largely via negative ion formation). If negative ions are not obtained, i.e., if there is no electron affinity, as in helium, no medium (vacuum) or if there is rapid ionization decay due to free radicals, there may be no visible or only a transient luminosity associated with the plasma even though it actually may be rich in free electrons.

H.   The Effect of Pressure on the Degree of Ionization in Gaseous Detonations

The results of this study were presented in item #11 of the list of technical notes. In recent years ionization in flames, shock waves, and in detonation waves has been the subject of a number of investigations. The Saha equation

$$\log k = \log [x/(1-x^2)p] = -5024\ E/T + 5/2\ \log T + \log g_i g_e/g_a - 6.47 \qquad (26)$$

(x is the fraction of the species ionized, p the pressure, E the ionization potential, T the absolute temperature, and g_i, g_e and g_a the statistical weights of the ion, electron, and atom, respectively) has been used to predict equilibrium constants for reactions of the type

$$A \rightleftharpoons A^+ + \epsilon^-$$

thus permitting calculations of electron densities in thermal ionization. As a general rule such calculations have yielded too low electron densities in flames. For detonations in condensed explosives, as already pointed out, the calculated values have been estimated to be too low by many orders of magnitude. On the other hand, for gaseous detonations in hydrogen-oxygen mixtures at relatively low pressure agreement was found between predictions based upon Saha's equation and experimental results, although at 50 atm deviations were beginning to become evident.

A large and important gap in experimental electron density results existed between the available measurements in low pressure gaseous detonations (50 atm or less) and results for condensed explosives where detonation pressures are up to 300 kb. The main purpose of this study was to bridge the gap as completely as possible by extending electron density measurements in gaseous detonations to as high pressures as possible and to determine the extent of departure from the thermodynamic equilibrium values predicted by Saha's equation.

One explanation for excess ionization as pressure is increased was based upon the quasi-lattice model. The cohesive energy resulting from such a structure should have the effect of lowering the effective ionization potential of the species in the detonation wave. Thus, as pressure or density increased the cohesive energy would increase and the ionization potential in turn would decrease, resulting in a greater degree of ionization than predicted by Saha's classical equation. Another explanation attributed the excess ionization to formation of hydrated ions, principally H_3O^+ which has been identified by mass spectrometers as an important ion in hydrogen-oxygen flames.

Electron density measurements were determined by the conduction probe method for the gaseous mixtures $2H_2 - O_2 - 0.002 N_2$, $2H_2 - O_2 - N_2$ and $2CO - O_2$. The pressure range covered was 9.55 to 347 atm, corresponding to initial pressures of 0.54 to 17.35 atm for the $2H_2 - O_2 - 0.002 N_2$ system, 17.3 atm to 313 atm, corresponding to initial pressures of 0.99 atm to 17.3 atm for the $2H_2 - O_2 - N_2$ system, and for $2CO - O_2$ the initial pressure was varied from 0.5 atm to 10 atm which corresponded to a detonation pressure range of 8.7 atm to 191 atm.

Thermohydrodynamic calculations were carried out for all the systems corresponding to the initial pressures of interest. Then the degree of ionization of each of the species was calculated using the equilibrium constants determined from Saha's equation. Due to the low ionization potential of NO it was essential that the concentration of N_2 be known accurately in each mixture. In the mixture $2H_2 - O_2 - 0.002 N_2$ the $0.002 N_2$ occurred as an impurity in the H_2, the actual concentration being determined by analysis with a mass spectrometer. For the hydrogen, oxygen, nitrogen mixtures the reactions leading to ionization which were first considered were

$$
\begin{aligned}
O_2 &\rightleftarrows O_2^+ + \epsilon^- \\
H_2O &\rightleftarrows H_2O^+ + \epsilon^- \\
NO &\rightleftarrows NO^+ + \epsilon^-
\end{aligned}
\tag{27}
$$

Ionization contributed by the other products of detonation H, O, H_2 and N_2 was negligible due to contributing factors of high ionization potential and low concentration of the species in the detonation products. The ionization contributing reactions considered in the $2CO - O_2$ system were

$$
\begin{aligned}
CO_2 &\rightleftarrows CO_2^+ + \epsilon^- \\
CO &\rightleftarrows CO^+ + \epsilon^- \\
O_2 &\rightleftarrows O_2^+ + \epsilon^- \\
O &\rightleftarrows O^+ + \epsilon^-
\end{aligned}
\tag{28}
$$

Comparisons were then carried out between the measured conductivities and theoretical conductivities based upon the calculated electron densities according to the reactions (27) or (28), and calculated electron mobilities. In the case of the oxygen-hydrogen-nitrogen mixtures, the theoretical and experimental conductivities were found to agree at the lowest pressures for which data were obtained.

For the $2CO - O_2$ system, however, the experimental conductivities exceeded the calculated conductivities by roughly 50 times. Thus, apparently some important ion contributing species must have been neglected in this system. For both the hydrogen-oxygen-nitrogen mixtures, as pressure was increased, the electrical conductivity was found to rise sharply above the theoretical curve calculated on the basis of H_2O^+, O_2^- and NO^+ formation, indicating therefore that an additional mechanism contributing ionization became important. Studies with mass spectrometers had revealed H_3O^+ to be an important ion species in hydrogen-oxygen flames, and since H_3O^+ formation would be expected to become more pronounced at high pressures, theoretical analyses were carried out to determine the influence upon electrical conductivity when H_3O^+ was considered.

An equilibrium constant for the reaction

$$H_2O^+ + H \rightleftharpoons H_3O^+ \tag{29}$$

was calculated from partition functions using an enthalpy of reaction, ΔH^O at $298^O K$ equal to -90 kcal/mole which was considered to be the best value available. This equilibrium constant turned out to be

$$K_{c37} = 0.197 \times 10^{-20}\ T^{-3/2}\ \epsilon^{44,840/T} = (H_3O^+)/(H_2O^+)(H)\ (molecules/cm^3)^{-1} \tag{30}$$

Reaction (29) was then considered simultaneously with reactions (27) and new electron densities and corresponding conductivities were calculated. Although the contribution to the total ionization by the formation of H_3O^+ increased with pressure, this contribution was much less than was required for agreement with experimental results. For example, at about 250 atmospheres using the $2H_2 - O_2 - 0.002\ N_2$ system inclusion of H_3O^+ in the theoretical calculations increased the degree of ionization only a negligible amount whereas approximately a tenfold increase was required.

In order to determine if the inclusion of H_3O^+ formation in the equilibria could possibly account for the sharp increase in the degree of ionization observed as pressure was increased above 20 atmospheres, a value of ΔH^O for the reaction given by equation (29) was chosen such that the calculated and experimental values of the conductivity agreed at 520 atm. This value of ΔH^O turned out to be -172.75 kcal/mole and the corresponding equilibrium constant was

$$K_{c37} = 0.197 \times 10^{-20}\ T^{-3/2}\ \epsilon^{86,300/T} \tag{31}$$

In this instance the calculations predicted much too high a degree of ionization for the low pressure region. Aside from the fact that $\Delta H^O = -172.72$ kcal/mole

certainly was an unacceptable value, the mechanism of H_3O^+ formation also proved unable to produce the observed shape of the electrical conductivity vs pressure curve.

The quasi-lattice model was then considered as a possible explanation of the excess ionization. In this model, provided the electron density is sufficiently large, the ions and electrons are considered to assume a quasi-metallic-like lattice structure in which the electrons move through the positive ion lattice in correlated patterns. Such a situation would lead to a cohesive energy, E_p, given approximately by the equation for metals

$$-E_p = BZ(1-0.8/dz^{4/5})/d \quad \text{(e.v. for d in Å)} \tag{32}$$

where d is the lattice distance, Z is the number of electrons per ion, and B is an emperical constant. This equation would, of course, apply only for situations where $-E_p$ was sufficiently greater than kT that the quasi-lattice structure was stable.

Due to the existence of cohesion, Saha's equation for thermionization was modified by subtracting from the E term the cohesive energy E_p, and calculations of the degree of ionization were carried out for the $2H_2 - O_2 - N_2$ system with the new, resulting equilibrium constants using various values of the emperical constant, B. Using the theroetical value of B equal to 30, which had been determined for metals, yielded a conductivity vs pressure curve that possessed the same shape as the experimental curve, but the electron densities predicted were too high. However, use of a value of B about 1/3 of this value gave good agreement throughout the whole range of pressures.

The sharp increase in conductivity with pressure observed in the hydrogen, oxygen, nitrogen systems was not found with $2CO - O_2$ contrary to expectations based upon the quasi-lattice model. However, in this case theoretical and experimental results proved to deviate widely even at low pressure. Thus, one did not have a reliable theoretical reference for low pressure from which to judge how theory and experiment deviated at high pressure.

I. Ionization and Electrical Conductivity and its Relationship to the Deflagration to Detonation Transition in Solid Explosives

At the preparing of this final report the investigations concerned with the above program are just being terminated and a technical note covering the study

will be prepared in the near future. Hence, only a description of the problem, its background, and a few of the results will be elucidated here.

The classical theory of detonation is based upon transport phenomena being negligible throughout the reaction zone. According to this theory a detonation wave is simply a shock wave supported by chemical reaction, the chemical reaction being initiated at the wave front by the Hugionot heat of compression of the shock wave. This theory predicts a pressure "spike" at the wave front whose magnitude is approximately twice the Chapman Jouguet pressure, which in the case of ideal explosives, is the pressure at the end of the reaction zone. The pressure at the wave front decays through the reaction zone at a rate proportional to the chemical reaction rate along the so-called Todes or Raleigh line.

Measurements of pressures at detonation wave fronts performed by this group under the auspices of another contract[7] negated the presence of a spike, however. The pressure at the detonation wave front was found not to exceed the Chapman Jouguet pressure. These determinations incidentally were performed for explosives possessing a wide variety of reaction zone lengths, the longer reaction zone lengths being sufficient that according to any existing theory a "spike" should have easily been discernable. Studies under still another contract[8] indicated, in fact, that the pressure exhibited a finite rise time at the front. According to the classical model, the temperature at the wave front would only be the order of several hundred degrees and thus the chemical reaction should be slow at first. This fact it would seem should lead to excessively long reaction times and a chemical induction period at the wave front.

The presence of the high electron densities in the detonation reaction zones as described earlier in the report, however, provided a mechanism whereby conduction of heat in the reaction zone could be considerable owing to the high mobility of electrons under the influence of a sharp thermal gradient at the wave front. Thus, conceivably appreciable amounts of heat could be conducted from within the reaction zone to the wave front, the effects of which would be to diminish magnitude of the "spike" erasing it completely if the heat conduction were sufficient, and to increase the temperature at the detonation wave front thereby increasing the chemical reaction rate at the front.

High electron densities and apparently high heat conduction therefore were existing conditions in detonation. The next question of interest was, naturally,

are they necessary conditions for detonation? This question prompted the initiation of the program with which this section is concerned. As a part of another investigation concerned with the transition to detonation for the shock initiation of liquid explosives in the so-called "card-gap" test, photographs showed a super velocity phenomenon of low luminosity starting at the barrier-receptor interface and terminating at the initial shock front with the transition to high order detonation occurring at the intersection of these two phenomena.[8] In line with the ideas of the importance of ionization in the detonation reaction zone this super velocity phemomena was interpreted to be a wave of ionization which cascaded to the shock front from the barrier receptor interface as a result of chemical reaction initiated by the initial shock wave and was termed the "flash across" or "heat pulse".

The studies with which this section pertains involved the measurements of conductivity for solid explosives initiated by shock in the "card gap" test and interpreting the relationship between conductivity and the deflagration to detonation transition. The measurements were made with the conduction probe method primarily in the region between the barrier-receptor interface and the distance, S_2, beyond it where high order detonation first occurred, both single sets and double sets of perpendicular probes as well as parallel probes being employed. The perpendicular probes were so-called because the conductors were perpendicular to the charge axis with the probe gap on the charge axis thus providing a measurement of conductivity vs time at one point within the charge for each set of probes. The parallel probe system, on the other hand, consisted of two conductors mounted symmetrically about and parallel to the charge axis, thus giving an integrated value of the conductivity between them. The main use of the double probe system was to verify in which direction (forward or backward) each of the disturbances propagated.

The investigations were commenced under the contract that this final report covers, namely Contract AF-18(603)-100. However, they continued into the present contract, AF-49(638)1061, and at present have reached the logical state where a technical note should be prepared soon. One of the most important results that was determined in this program was confirmation of the "flash across" mechanism. In the transition state before high order detonation has been established the

ionization wave was found to exhibit a long, gradual rise. The ionization started apparently at the pressure front but during the initial stages the rise time of the ionization wave was much longer than the rise time of the initial pressure wave. However, as the disturbance propagated through the donor charge the ionization wave was found to sharpen, and after the ionization wave had sharpened to a steep fronted wave which coincided apparently with the initial pressure wave the transition to high order detonation occurred. In other words, the transition took place when the ionization front merged with the shock front permitting conduction of heat to the shock front. One would expect that a critical amount of ionization would be required before the associated luminosity would be sufficient for photography. Thus, the super velocity "flash across" phenomenon observed in liquids probably corresponded to the propagation of a critical level of ionization. The velocity associated with it would be considerably greater than the velocity of the initial pressure wave as a result of the "sharpening up" of the ionization wave.

J.   Transition to Detonation in Liquid Explosives

As mentioned in the previous section a super velocity, slightly luminous phemomenon has been observed to start at the barrier-receptor interface and propagate to the initial shock front at which point normal high order detonation is established. The interpretation advanced at this laboratory was that the phemomenon was not of a "hydrodynamic" nature but corresponded to a critical level of ionization which by virtue of the chemical reaction started by the initial shock and by heat conduction, cascaded to the initial shock front, high order detonation occurring when the ionization wave with its associated high conductivity merged with the initial shock. Another explanation has been advanced for this phenomenon, [9,10] namely that the super velocity phenomenon is a high order detonation which starts at the barrier-receptor interface propagating at super detonation velocity to the shock front by virtue of the high density of the compressed medium between the initial shock front and the barrier. This explanation required that the mechanism of shock initiation is different in liquid than in solids for which the transition to detonation occurs some distance within the receptor. A crucial experiment which would determine whether or not the latter explanation is correct is the measurement of the pressure associated with the super velocity phenomenon. If it were indeed a detonation the pressure would be exceedingly high, having a value several times the normal

detonation pressure of the liquid, whereas if it were an ionization phenomenon, the pressure would be lower than the pressure of the initial shock.

The task of measuring the pressure associated with the hypervelocity phenomenon in liquids was undertaken during the latter part of the contract period, and the investigations are being continued under the auspices of the new contract. The only method of estimating the pressure which would appear to give valid results is the aquarium technique in which the shock is transmitted into an inert medium of known equation of state. The use of such a method requires especially careful techniques in this case. The transition to detonation or the overtaking of the initial shock by the detonation wave that started at the plate, whichever the case may be, should occur slightly inside pressure measuring medium (imagining that the pressure measuring medium were the same as the explosive). Hence, it is important that the shock impedance of the explosive match the impedance of the transmitting medium in order that reflections do not occur at the interface which might influence the transition. Also, it is necessary that distance from the barrier at which the coelescence occurs be known accurately so that the proper length of receptor charge be known. If, then, the hypervelocity phenomenon is a detonation, a strong shock velocity "overshoot" must be measured in the transmitting medium.

At the end of the contract period positive results had not been obtained. However, the S_1 vs S_2 relationships, where S_1 is the barrier thickness and S_2 is the distance beyond the barrier at which the hypervelocity phenomenon and the initial shock front merged, had been determined for nitromethane using a particular charge geometry, and a transmitting medium whose equation of state was a good match for NM has been found. During the new contract period efforts will be devoted to this problem through studies with a number of liquids. Determination of the correct interpretation of the "flash across" phenomenon would be an exceedingly important contribution to the theory of detonation.

BIBLIOGRAPHY

1. M. A. Cook, Discussions of Faraday Society, No. 22, Paper No. 25, Glasgow, September 20, 21, 1956.

2. R. J. Eichelberger, J. Appl. Phys., 27, 63 (1956); also report entitled "Re-examination of Theories of Jet Formation and Penetration of Fluid Cavity Charges", Carnegie Institute of Technology, Dept. of Physics., CEL Report #1, June 1954.

3. M. A. Cook, Bulletin No. 52, 422, September 21, 1951, Utah Engineering Experiment Station, University of Utah.

4. H. Eyring, R. E. Powell, G. H. Duffey, and R. B. Parlin, Chem. Rev., 45, 16 (1949).

5. H. Jones, Roy. Soc. Proc. (London) A189, 415 (1947); see also J. L. Copp and A. R. Ubbelohde, Faraday Soc. Trans. 44, 646 (1948).

6. M. A. Cook, "The Science of High Explosives", ACS Monograph Series, Reinhold Publishing Corporation, New York (1958).

7. M. A. Cook, R. T. Keyes, and W. O. Ursenbach, "Measurements of Shock and Detonation Pressures", Contract NOw 61-0411-d, Institute of Metals and Explosives Research, University of Utah, April 28, 1961.

8. M. A. Cook, W. A. Gey, and D. H. Pack, "Transition from Deflagration to Detonation in Solid Propellants", Technical Report #3, Contract N123(60530)8011A, Institute of Metals and Explosives Research, University of Utah, December 15, 1958.

9. R. F. Chaiken, "Comments on Hypervelocity Wave Phenomena in Condensed Explosives", p. 304, Third ONR Symposium on Detonation, Princeton University, September 1960.

10. H. W. Campbell, W. C. Davis, and J. R. Travis, "Shock Initiation of Detonation in Liquid Explosives," ibid, p. 469.

DISTRIBUTION LIST

	No. of copies		No. of copies
Commander AF Office of Scientific Research ATTN: SRY Washington 25, D. C.	3	Armed Services Technical Info. Agency ATTN: TIPCR Arlington Hall Station Arlington 12, Virginia	10
Commander AF Research Division ATTN: RRRTL Washington 25, D. C.	2	Director of Research and Development Headquarters, USAF ATTN: AFDRD Washington 25, D. C.	1
Commander Wright Air Development Division ATTN: WWAD Wright-Patterson Air Force Base Ohio	4	Office of Naval Research Department of the Navy ATTN: Code 420 Washington 25, D. C.	1
Commander AF Cambridge Research Laboratories ATTN: CRREL L. G. Hanscom Field Bedford, Massachusetts	1	Director, Naval Research Laboratory ATTN: Technical Information Officer Washington 25, D. C.	1
Commander Rome Air Development Center ATTN: RCOIL-2 Griffiss Air Force Base Rome, New York	1	Director, Army Research Office ATTN: Scientific Information Branch Department of the Army Washington 25, D. C.	1
Commander Detachment 1 Hq AF Research Division The Shell Building Brussels, Belgium	2	Chief, Physics Branch Division of Research U.S. Atomic Energy Commission Washington 25, D. C.	1
P. O. Box AA Wright-Patterson Air Force Base Ohio	1	U.S. Atomic Energy Commission Technical Information Extension P. O. Box 62 Oak Ridge, Tennessee	1
Aeronautical Research Laboratories ATTN: Technical Library Building 450 Wright-Patterson Air Force Base Ohio	1	National Bureau of Standards Library Room 203, Northwest Building Washington 25, D. C.	1
Director, Department of Commerce Office of Technical Services Washington 25, D. C.	1	Physics Program National Science Foundation Washington 25, D. C.	1
		Director, Office of Ordnance Research Box CM, Duke Station Durham, North Carolina	1

ARO, Inc.
ATTN: AEDC Library
Arnold Air Force Station
Tullahoma, Tennessee   1

Commander
AF Flight Test Center
ATTN: FTOTL
Edwards Air Force Base
California   1

Commander
AF Special Weapons Center
ATTN: SWOI
Kirtland Air Force Base
New Mexico   1

Commander
AF Missile Development Center
ATTN: HDOI
Holloman Air Force Base
New Mexico   1

Commander
Army Rocket & Guided Missile Agency
ATTN: ORDXR-OTL
Redstone Arsenal
Alabama   1

Commandant
Air Force Institute of Technology
(AU) Library
MCLI-LIB, Bldg. 125, Area A
Wright-Patterson Air Force Base
Ohio   1

Commander
Air Research and Development Command   2
ATTN: RDR   1
        RDRB   1
        RDRC   1
        RDRS
Andrews Air Force Base
Washington 25, D. C.

Rand Corporation
1700 Main Street
Santa Monica, California   1

Commanding General
U.S. Army Signal Corps Research
  and Development Laboratory
ATTN: SIGFM/EL-RPO
Ft. Monmouth, New Jersey   1

National Aeronautics & Space
  Administration
Washington 25, D. C.   6

Advanced Research Projects Agency
Washington 25, D. C.   1

Chairman
Canadian Joint Staff
for DRB/DSIS
2450 Massachusetts Ave., N.W.
Washington 25, D. C.   1

Commander
Air Proving Ground
ATTN: ACOT
Eglin Air Force Base
Florida   1

Commander
Wright Air Development Center
ATTN: WCRTM-1
Wright-Patterson Air Force Base
Ohio   1

Director, Office of Naval Research
Chicago Branch Office
86 East Randolph Street
Chicago 1, Illinois   1

Commanding Officer
Aberdeen Proving Ground
ATTN: Terminal Ballistic Lab.   1
      WSL   1
Aberdeen, Maryland

Institute for Air Weapons Research
Museum of Science and Industry
University of Chicago
Chicago 37, Illinois   1

Armour Research Foundation
33 West 33rd Street
Illinois Institute of Technology
Chicago, Illinois   1

Commanding Officer
Frankford Arsenal
Attn: Director, Pitman-Dunn Lab
Philadelphia 37, Pennsylvania   1

Commanding Officer
Picatinny Arsenal
Attn: Technical Division
Dover, New Jersey   1

Chief, Bureau of Naval Weapons
Research and Development Division
Department of the Navy
Washington 25, D. C.   1

Commanding Officer
U.S. Naval Ordnance Test Station
Attn: Technical Library
Inyokern, China Lake, California   2

Dr. P. Whitman
Applied Physics Laboratory
Johns Hopkins University
Silver Spring, Maryland   1

Mr. H. W. Wells
Carnegie Institution of Washington
Department of Terrestrial Magnetism
5241 Broad Branch Road, N.W.
Washington 15, D. C.   1

Stanford Research Institute
Poulter Laboratories Document Custodian
Menlo Park, California   1

U.S. Department of the Interior
Bureau of Mines
4800 Forbes Avenue
Pittsburgh 13, Pennsylvania
Attn: M. P. Benoy, Reports Librarian
        Division of Explosives
          Technology   1

Applied Mechanics Reviews
South West Research Institute
8500 Culebra Road
San Antonio 6, Texas   1

National Bureau of Standards
Plastics Section
Attn: Dr. Olive Engel
Washington 25, D. C.   1

National Bureau of Standards
Boulder Laboratories
Boulder, Colorado   1

Dr. E. Paul Palmer
Ramo-Wooldridge Corporation
Guided Missile Division
P. O. Box 45564
Air Port Station
Los Angeles 45, California   1

Commander
U.S. Naval Proving Ground
Attn: Warhead and Terminal Ballistics
       Lab., Research Division
Dahlgren, Virginia   1

Institute of the Aeronautical Sciences
Attn: Librarian
2 East 64th Street
New York 16, New York   1

Colorado School of Mines
Attn: J. S. Rinehart
Golden, Colorado   1

Commanding Officer
U.S. Naval Propellant Plant
Attn: Technical Library
Indian Head, Maryland   1